

# The piezoelectric response of electrospun PVDF nanofibers with graphene oxide, graphene, and halloysite nanofillers: a comparative study

Mina Abbasipour<sup>1</sup> · Ramin Khajavi<sup>2</sup> · Ali Akbar Yousefi<sup>3</sup> ·  
Mohammad Esmail Yazdanshenas<sup>4</sup> · Farhad Razaghian<sup>5</sup>

Received: 3 May 2017 / Accepted: 5 July 2017 / Published online: 15 July 2017  
© Springer Science+Business Media, LLC 2017

**Abstract** Although, many efforts were performed to develop piezoelectric systems with high energy conversion rate, but they still show insufficient performance. In this study, the effect of three nanofillers with different morphology and their concentration on macro/micro structure and piezoelectric properties of polyvinylidene fluoride (PVDF) nanofibers were investigated and compared. Graphene oxide (GO) and graphene (Gr) as planner nanofillers, and halloysite (Hal) nanotube were introduced into a PVDF solution in different concentrations (0.05–3.2 wt/wt%). The prepared solutions were fabricated into nanofibers through electrospinning method. The electroactive phase ( $\beta$ -phase) of nanofibrous PVDF mat increased up to ~49% in comparison with PVDF powder. The presence of nanofiller in PVDF matrix also increased it more up to 10%. Gr nanofiller had least effect on piezoelectric properties attributed to its low interaction with PVDF chains. PVDF/Hal nanocomposite with low filler content concentration (<0.1 wt

wt%) and PVDF/GO with high content of filler concentration (>0.4 wt/wt%) caused higher polar phase. Hal nanotubes with a rod like morphology caused more oriented and finer nanofibers than PVDF/GO and PVDF/Gr nanofibers. However, PVDF/0.8 Hal showed higher output voltage (0.1 V), despite of its lower  $\beta$ -phase in compared with PVDF/0.8GO nanocomposites. It was concluded that the piezoelectric response cannot be just evaluated with dielectric constant of nanofiller or  $\beta$ -phase percentage in an electrospun PVDF nanocomposite, but there are some other important factors like orientation and fineness of electrospun nanofibers.

## 1 Introduction

Piezoelectric materials are being used for sensors, actuators, and energy harvesting applications progressively [1]. They are categorized into two main groups: ceramics (PZT and BaTiO<sub>3</sub>) and polymers (mainly PVDF (CH<sub>2</sub>-CF<sub>2</sub>)<sub>n</sub>). Although piezoelectric ceramics have high piezoelectricity properties, they are toxic, brittle, and inflexible. In contrast, polymeric piezo-materials, such as electroactive PVDF polymers, offer flexibility, which makes them easy to shape. PVDF can be crystallized into five different polymorphisms ( $\alpha$ ,  $\beta$ ,  $\gamma$ ,  $\delta$ , and  $\epsilon$ ) related to chain conformation (T=trans, G=gauche). The non-polar and paraelectric  $\alpha$ -phase with TGTG conformation is the most frequent occurring polymorph because of its high thermodynamic stability at ambient temperature and pressure. However, the most welcome polymorph is the  $\beta$ -phase; it has an all trans (TTTT) conformation, which shows significant piezoelectricity that corresponds to its highest dipolar moment. The piezoelectric property is dependent on the  $\beta$ -phase's amount of the PVDF polymer or its total crystallinity [1, 2]. This phase

**Electronic supplementary material** The online version of this article (doi:10.1007/s10854-017-7491-4) contains supplementary material, which is available to authorized users.

✉ Ramin Khajavi  
rkhajavi@gmail.com

<sup>1</sup> Department of Textile Engineering, Science and Research Branch, Islamic Azad University, Tehran, Iran

<sup>2</sup> Department of Polymer and Textile Engineering, South Tehran Branch, Islamic Azad University, Tehran, Iran

<sup>3</sup> Faculty of Polymer Processing, Iran Polymer and Petrochemical Institute, Tehran, Iran

<sup>4</sup> Department of Textile Engineering, Yazd Branch, Islamic Azad University, Yazd, Iran

<sup>5</sup> Department of Electrical Engineering, South Tehran Branch, Islamic Azad University, Tehran, Iran

can be induced or improved by mechanical stretching [3–10], poling [11, 12], thermal annealing [13–16], electrospinning [17–20], and filler addition [21–23].

Electrospinning is a method for fabrication of PVDF nanofibrous mat (nanofibers) and inducing  $\beta$ -phase simultaneously. The presence of an electrical field and stretching forces in this method would result to dipoles alignment such that the non-polar  $\alpha$ -phase is transformed into the polar  $\beta$ -phase [18]. There are many papers for fabrication, evaluation, and improvement of piezoelectric nanofibers through electrospinning method. For example, Wang et al. [24] and Chang et al. [25, 26] have evaluated the output voltage of electrospun PVDF nanofibers for sensing and nanogenerator application. Shao et al. [27] and Gheibi et al. [28] investigated the effects of PVDF concentration and electrospinning parameters, such as applied voltage and spinning distance, as well as the nanofibers' mat thickness on  $\beta$ -phase content and mechanical to electrical energy conversion properties. Gheibi et al. [29] determined that electrospun PVDF nanofibers can produce a 1 V output, which can be used for a wearable self-powered electrical device. Fang et al. [30, 31] obtained an output of 2 V in 1 Hz and 8 V in 10 Hz, with an output current of 4  $\mu$ A for randomly oriented and needless electrospun PVDF nanofibers.

Filler addition to PVDF matrix has been used for improving the  $\beta$ -phase formation and various nanofillers have been introduced up to now. The most used nanofillers are carbon nanotubes [32–35], Ag nanowires [36], clay [37–39], ZnO [40], and graphene [41–45]. Yousefi [46] introduced both the Cloisite 30B and multiwall carbon nanotube (MWCNT) into the PVDF matrix to enhance the  $\beta$ -phase by up to 80%. Cho et al. [47] studied the effects of  $\text{NH}_2$ -treated graphene nanodot/reduced GO nanocomposites on crystalline structures of PVDF and they improved  $\beta$ -phase. Thakur et al. [48] found that Hal enhanced the  $\beta$ -phase as well as the dielectric constant of PVDF film. Huang et al. [49] incorporated GO in PVDF nanofibers to increase the output voltage of the triboelectric nanogenerator. Jiang et al. [50] concluded that the combination of a chemical addition and a mechanical deformation promotes the  $\beta$ -phase in PVDF, which further enhances its piezoelectric properties.

There are some studies presenting the effects of fillers for enhancing piezoelectric properties of PVDF. For example, Fakhri et al. [51] made PVDF based nanocomposites containing GO/Au and GO/Cu fillers by solution casting. They resulted that both fillers improved the electroactive phases and caused a high dielectric constant accompanied with low dielectric loss in compare to pure PVDF film. In another study, Mokhtari et al. [52] compared the effect of different additives including ZnO, CNT, LiCl, and PANI. CNT lead to more  $\beta$ -phase formation and higher output voltage in comparison with other additives. However,

there is no study to investigate the effect of important filler properties like conductivity and the morphology on the piezoelectric properties of PVDF nanofibers. Furthermore, there is no study to compare different nanofillers with each other with respect to these characteristics for PVDF in the nanofibrous form.

To investigate filler properties especially morphology on the piezoelectric response of electrospun PVDF nanocomposite, GO, Gr (as planner nanofillers) and Hal nanotube were selected due to their wide applications in electronics devices [53–55]. PVDF solved in DMF/acetone (6:4 v/v) and GO, Gr, and Hal nanotube in different concentrations were added and fabricated into nanofibrous mat by electrospinning method. The effects of nanofillers on the transition phase and the dielectric and piezoelectric properties of the PVDF polymer were systematically investigated by Fourier transform infrared spectroscopy (FTIR), differential scanning calorimetry (DSC), X-ray diffraction (XRD), LCR meter, and oscilloscope. The  $\beta$ -phase formation, dielectric constant, and piezoelectricity were enhanced by the addition of fillers. The new finding of this paper is existence of some other important factors like orientation and fineness of electrospun nanofibers on piezoelectric response over dielectric constant of nanofiller or  $\beta$ -phase percentage.

## 2 Experimental

### 2.1 PVDF nanofibers fabrication

A high voltage electrospinning technique was used to produce PVDF ( $M_w \approx 534,000$ , Sigma Aldrich) in nanofibrous form. Nanofibers were electrospun from PVDF solution (14 wt/v%) dissolved in a solvent mixture of DMF/acetone (6:4 v/v) with different content of GO (99%, 3.4–7 nm, 6–10 layers, US Research Nanomaterials, USA), Gr nanosheets (99.5%, 2–18 nm, less than 32 layers, US Research Nanomaterials, USA) and Hal nanotubes (diameter=30–70 nm, length=2–3  $\mu$ m, Sigma Aldrich) (0.05, 0.1, 0.2, 0.4, 0.8, 1.6 and 3.2 wt%; Table 1). The processing parameters were

**Table 1** Samples code

Nanofiller content (wt/wt%)	Graphene oxide	Graphene	Halloysite
0.05	0.05GO	0.05Gr	0.05Hal
0.1	0.1GO	0.1Gr	0.1Hal
0.2	0.2GO	0.2Gr	0.2Hal
0.4	0.4GO	0.4Gr	0.4Hal
0.8	0.8GO	0.8Gr	0.8Hal
1.6	1.6GO	1.6Gr	1.6Hal
3.2	3.2GO	3.2Gr	3.2Hal

kept the same for all samples (feeding rate = 2 ml/h, rotating drum speed = 300 rpm, needle = 20 G, tip-to-collector distance = 100 mm, and the applied voltage = 16 kV). The nanofillers were sonicated with an ultrasonic probe (100 W, 40 kHz, 15 min, Heidolph, Germany) before and after adding to polymer matrix.

## 2.2 Characterizations

Morphology and diameter of produced nanofibrous mats were observed by scanning electron microscopy (SEM, Tescan, Vega model, Czech Republic) and ImageJ software®.

Their crystalline characteristics of samples and  $\beta$ -phase formation were determined by X-ray diffraction (XRD, Bruker D8 X-ray diffractometer, Germany) using Cu-K $\alpha$  radiation from  $2\theta = 10^\circ$ – $40^\circ$  at 1 s per step of  $0.02^\circ$ . The relative proportion of the XRD peaks for  $\beta$ -phase was estimated by the peak intensities of (200/110), (100), (020), (110), and (021) as Eq. (1) [47]:

$$\frac{I_\beta}{I_\alpha + I_\beta} = \frac{I_{200/110}}{(I_{100} + I_{020} + I_{110} + I_{021})_\alpha + (I_{200/110})_\beta} \quad (1)$$

In Eq. (1) the  $I_{100}$ ,  $I_{020}$ ,  $I_{110}$ ,  $I_{021}$  and  $I_{200/110}$  are the peak intensity at (100), (020), (110), (021), and (200/110) planes, respectively. The heights that correspond to these peaks were analyzed with peak analyzer software (Origin software-version 94E, Evaluation).

To analyze the crystallization behaviors of the PVDF nanocomposites nanofibers further, the differential scanning calorimetry (Setaram, DSC 131, France) thermograms of the PVDF composite nanofibers were obtained with a heating rate of  $10^\circ\text{C min}^{-1}$  and a cooling rate of  $8^\circ\text{C min}^{-1}$  from 0 to  $200^\circ\text{C}$ . The crystallinity degree ( $X_c$ ) of PVDF composite nanofibers was calculated by Eq. (2):

$$X_c = \frac{\Delta H_m}{\Delta H_{100\%}} \times 100 \quad (2)$$

where  $\Delta H_m$  and  $\Delta H_{100\%}$  refer to the heat of fusions of sample and 100% crystalline (104.7 J/g) [48].

Fourier transform-infrared (FT-IR, ATR mode) spectra were obtained with Bruker, IFS48. The fraction of  $\beta$ -phase [ $F(\beta)$ ] in different samples was calculated from IR spectra using Lambert–Beer law according to Eq. (3):

$$F(\beta) = \frac{A_\beta}{\left(\frac{K_\beta}{K_\alpha}\right)A_\alpha + A_\beta} \quad (3)$$

where  $A_\alpha$  and  $A_\beta$  are the absorbance at  $764$  and  $840\text{ cm}^{-1}$ , respectively and  $K_\beta$  ( $7.7 \times 10^4\text{ cm}^2\text{ mol}^{-1}$ ) and  $K_\alpha$  ( $6.1 \times 10^4\text{ cm}^2\text{ mol}^{-1}$ ) are the absorption coefficients at the

respective wavenumber [48]. The heights that correspond to these peaks were analyzed with peak analyzer software (Origin software-version 94E, Evaluation).

Raman spectroscopy (Thermo-Nicolet FT Raman 960, USA) was used to study the changes of GO and Gr layers in combination with polymeric chains as well as their influence on the PVDF structure.

The dielectric properties, resistivity and impedance were measured by using a LCR meter (GW Instek, LCR 817). The dielectric constant ( $\epsilon$ ) of the samples was calculated using Eq. (4):

$$\epsilon = C \cdot d / \epsilon_0 A \quad (4)$$

where  $C$ ,  $d$  and  $A$  are the capacitance, thickness and area of the samples, respectively and  $\epsilon_0$  is the permittivity of free space with a value  $8.854 \times 10^{-12}\text{ F m}^{-1}$  [48].

## 2.3 Power-generator nanofibrous modulus

The power-generating sample was assembled using a square piece of nanofibrous web ( $35\text{ cm}^2$ ), aluminum foils as electrodes, a spacer (paper), and a polycarbonate sheet (thickness = 0.3 mm). A compression force of 0.49 N with a frequency of 2 Hz was applied on power-generating sample. Finally, the output voltage and current were recorded by an oscilloscope (Instek GDS-1072). To ensure the appropriate piezoelectric properties and calibration, a modulus with a paper sheet—instead of a PVDF layer and an earth connection—were used to set the voltage equal to zero.

## 2.4 Piezoelectric properties

The piezoelectric voltage coefficient ( $g$ ) relates the electric field generated by an applied mechanical stress and can be measured by the Eq. (5):

$$g_{33} = V_{2wt} / 3F_3 l \quad (5)$$

where ‘ $V$ ’ is the maximum voltage generated, ‘ $w$ ’ is the width, ‘ $t$ ’ is the thickness, ‘ $l$ ’ is the length of the piezoelectric material and ‘ $F$ ’ is the force applied. The piezoelectric voltage constant is an important parameter for assessing the material suitability [56].

The piezoelectric coefficient  $d_{33}$  was measured as Eq. (6):

$$d_{33} = Q/F = C_m V_m / F \quad (6)$$

where  $F$  is applying force and  $Q$  is an electric charge which measured as a voltage  $V_m$  over a capacitor ( $C_m = 3\text{ }\mu\text{F}$ ) in parallel with the sample [57].

As Eq. (7), figure of merit of samples ( $FOM_{33}$ ) were calculated from the piezoelectricity ( $d_{33}$ ) and the piezoelectric voltage coefficient ( $g_{33}$ ) [58].

$$FOM_{33} = g_{33} \times d_{33} \tag{7}$$

### 3 Results and discussion

#### 3.1 Microstructure characterization

The average diameter of electrospun pristine PVDF nanofibers was measured about 140 nm (Fig. 1a). Whereas, for PVDF/(0.2 & 0.8 wt%)GO, PVDF/(0.2 & 0.8 wt%) Gr and PVDF/(0.2 & 0.8 wt%)Hal nanofibers the average diameter increased and reached to (180 & 340 nm), (170 & 210 nm) and (150 & 190 nm), respectively (Fig. 1b–d). Adding nanofillers to a polymer matrix usually increases the viscosity and consequently thicker nanofibers formed [50, 57]. The mean diameter of GO and Gr samples showed higher values in compare with Hal samples which is attributed to high specific surface area of them. Increasing the nanofiller content by 0.8 wt% caused the diameter of Gr and Hal to increase for about 40 nm, but for GO the increase was larger and reached to 340 nm. As it can be seen from Fig. 1h the slope of GO line is higher than Hal and Gr samples due to higher interactions caused by hydroxyl and carboxyl groups of GO nanosheets [57]. Moreover, Fig. 1f, g shows that the ribbon-like nanofibers formed. The nanofibers orientation was

analyzed with Image j software (orientation j). The coherency indicates if the local image features are oriented or not: C is 1 when the local structure has one dominant orientation and C is 0 if the image is essentially isotropic in the local neighborhood. Higher values of coherency show that nanofibers aligned in unique direction. It was found that the Hal samples had higher orientation than GO samples (Table 2).

#### 3.2 Crystal polymorphism

The FTIR spectra of the PVDF nanofibers with different amounts of filler are shown in Fig. 2a. The FTIR spectrum of the GO represented bands at 1038 (C–O stretching), 1157 (C–O–C stretching). The oxygen-containing functional group of GO is represented in bands at 1356 and 1718  $\text{cm}^{-1}$ , corresponding to the C–O–H deformation

**Table 2** Nanofibers orientation and coherency

Sample	Orientation (°)	Coherency
PVDF	51.37	0.097
0.2GO	-76.33	0.059
0.2Gr	83.98	0.065
0.2Hal	-85.12	0.086
0.8GO	81.59	0.085
0.8Gr	-81.61	0.067
0.8Hal	58.07	0.13

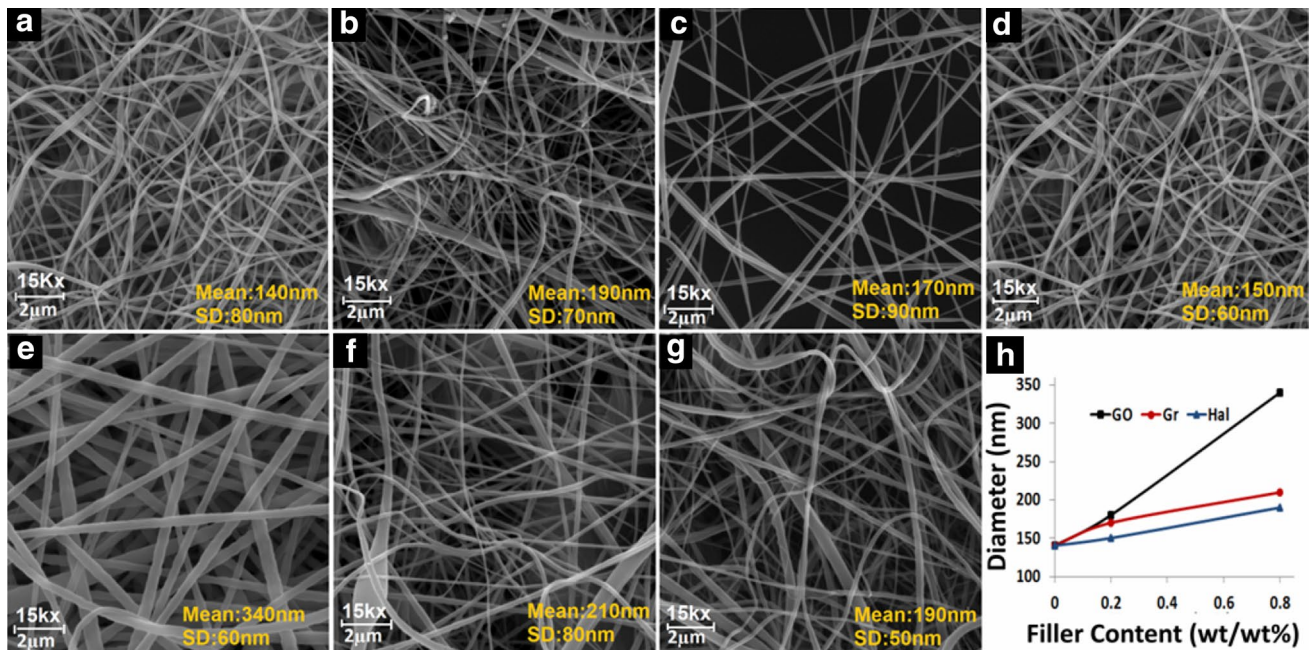


**Fig. 1** SEM micrograph of samples. Morphology and size distribution of **a** pure PVDF, **b** PVDF/0.2 wt%GO, **c** PVDF/0.2 wt%Gr, **d** PVDF/0.2 wt% Hal, **e** PVDF/0.8 wt%GO, **f** PVDF/0.8 wt% Gr and **g** PVDF/0.8 wt% Hal



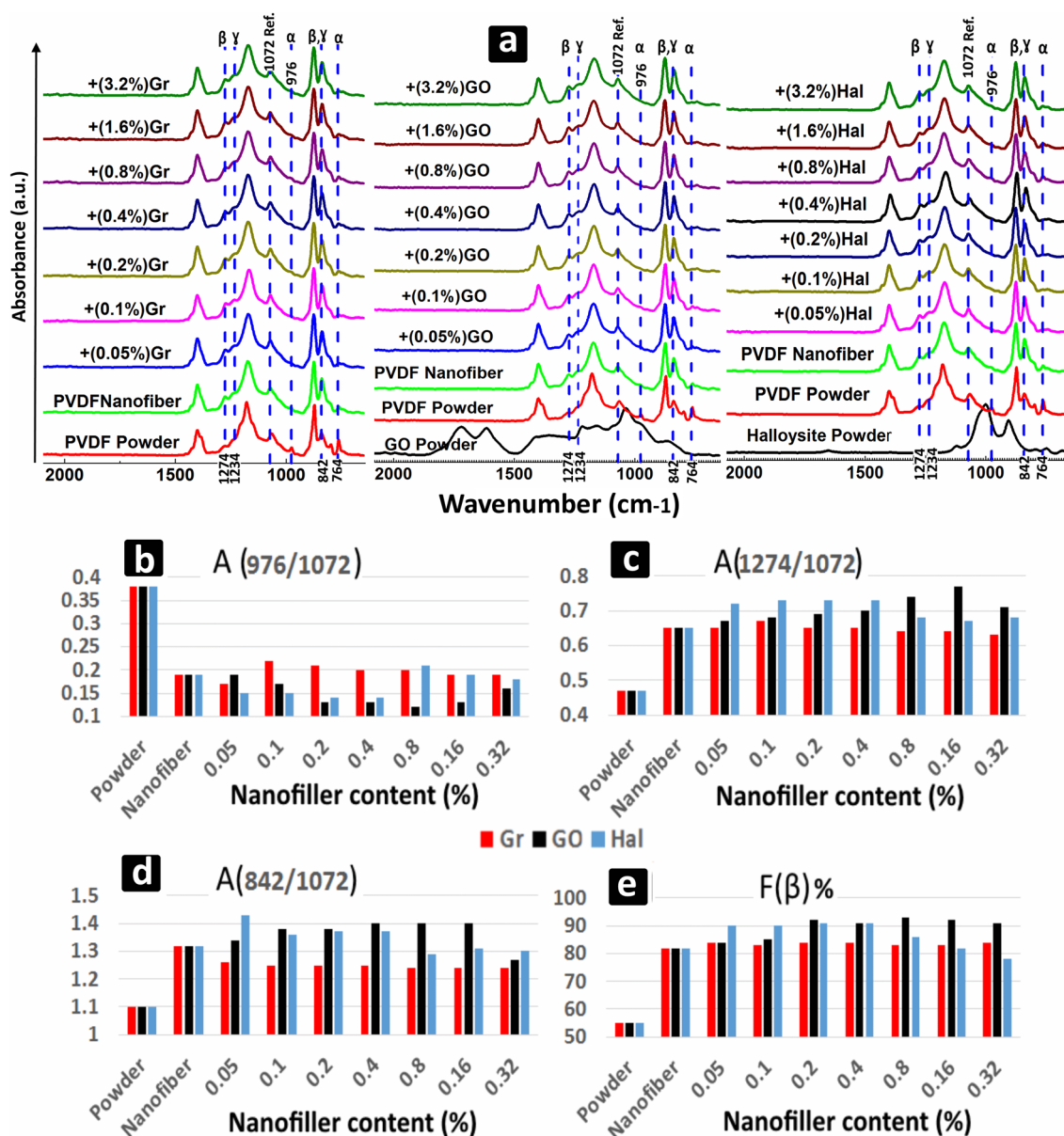


**Fig. 2** a FTIR, b  $\alpha$  and c–e  $\beta$ -phase of samples with different content of nanofillers

and C=O stretching of the COOH groups, respectively. The peak at  $1615\text{ cm}^{-1}$  in the GO represents the skeletal vibration of unoxidized graphitic domains [47]. Several absorption bands at 764, 976, and  $978\text{ cm}^{-1}$  were ascribed to the  $\alpha$ -phase of the PVDF, and the absorption bands for the  $\beta$ -phase appeared at 842 and  $1272\text{ cm}^{-1}$ . After the addition of fillers, the peaks assigned to the  $\beta$ -phase became significantly stronger and sharper, while the peaks corresponding to the  $\alpha$ -phase became indistinctive. Another band at  $1234\text{ cm}^{-1}$  can be seen as well, which also seems to be characteristic of the  $\gamma$ -phase [57]. The relative fraction of the  $\beta$ -phase in samples  $[F(\beta)]$  was calculated using Eq. (1), and variation of the percentage of  $F(\beta)$  with filler

content (wt%) is graphically represented in Fig. 2e. It also shows that the  $\alpha$ -phase decreased dramatically by altering the PVDF powder to nanofiber forms; however, the  $\beta$ -phase formation increased (Fig. 2c, d). For example, the  $\alpha$ -phase, ( $A_{976}/A_{1072}$ ) from 0.39 for the PVDF powder, decreased to 0.19 for the nanofiber. The  $\alpha$ -phase reduced 15 and 10% less than the pristine PVDF nanofiber for PVDF/(0.1 wt%) Gr and PVDF/(0.8 wt%) Hal, respectively, (Fig. 2b). The  $F(\beta)$  increased by approximately 8% more than the pristine PVDF nanofiber sample for concentrations of up to 0.2 wt% of GO and 0.05, 0.1, 0.2, and 0.4 wt% of Hal, while the  $F(\beta)$  of the Gr samples remained constant. PVDF/Hal nanocomposite with low filler content concentration

(<0.1 wt/wt%) and PVDF/GO with high content of filler concentration (>0.4 wt/wt%) caused higher polar phase. This is because of Hal nanotube has rod like structure which cause PVDF chains oriented easily along the electro-spinning direction [59]. The  $F(\beta)$  of the PVDF/Hal samples with concentration up to 0.4 wt% (Fig. 2e) increased. This may have been due to an increase in charge accumulations at the interfaces of the PVDF and the nanofillers, which resulted in a depolarization field exceeding the coercive field in nanocomposite fillers with nanofiller concentrations of >0.2 wt%. This would therefore cause a decrease in the efficiency of the polling process [60]. The use of GO, Gr, and Hal as nanofillers provided effective dipole polarization in the PVDF matrix and facilitated the nucleation of

$\beta$ -phase crystals due to the enhanced dipole–dipole forces. Graphene possesses a carbon atom with a zigzag structure, which matches the zigzag structure of the  $\beta$ -phase [60]. The attachment of PVDF chains to the GO sheets was caused by interaction between  $CF_2$  in PVDF and the  $-C=O$  and  $COOH$  groups of the GO (hydrophilic interaction) [61]. In the case of Hal, the negatively charged surface ( $SiO_2$ ) and  $OH$  interacted with  $CH_2$  in the PVDF chain [48]. In addition, the added nanofillers acted as a nucleating agent for the  $\beta$ -phase and as a hindering agent for the  $\alpha$ -phase [62].

Raman spectroscopy was used for further study of the changes of GO and Gr layers in combination with polymeric chains and their corresponding influence on the PVDF structure (Fig. 3a). Both 1331–1352  $cm^{-1}$

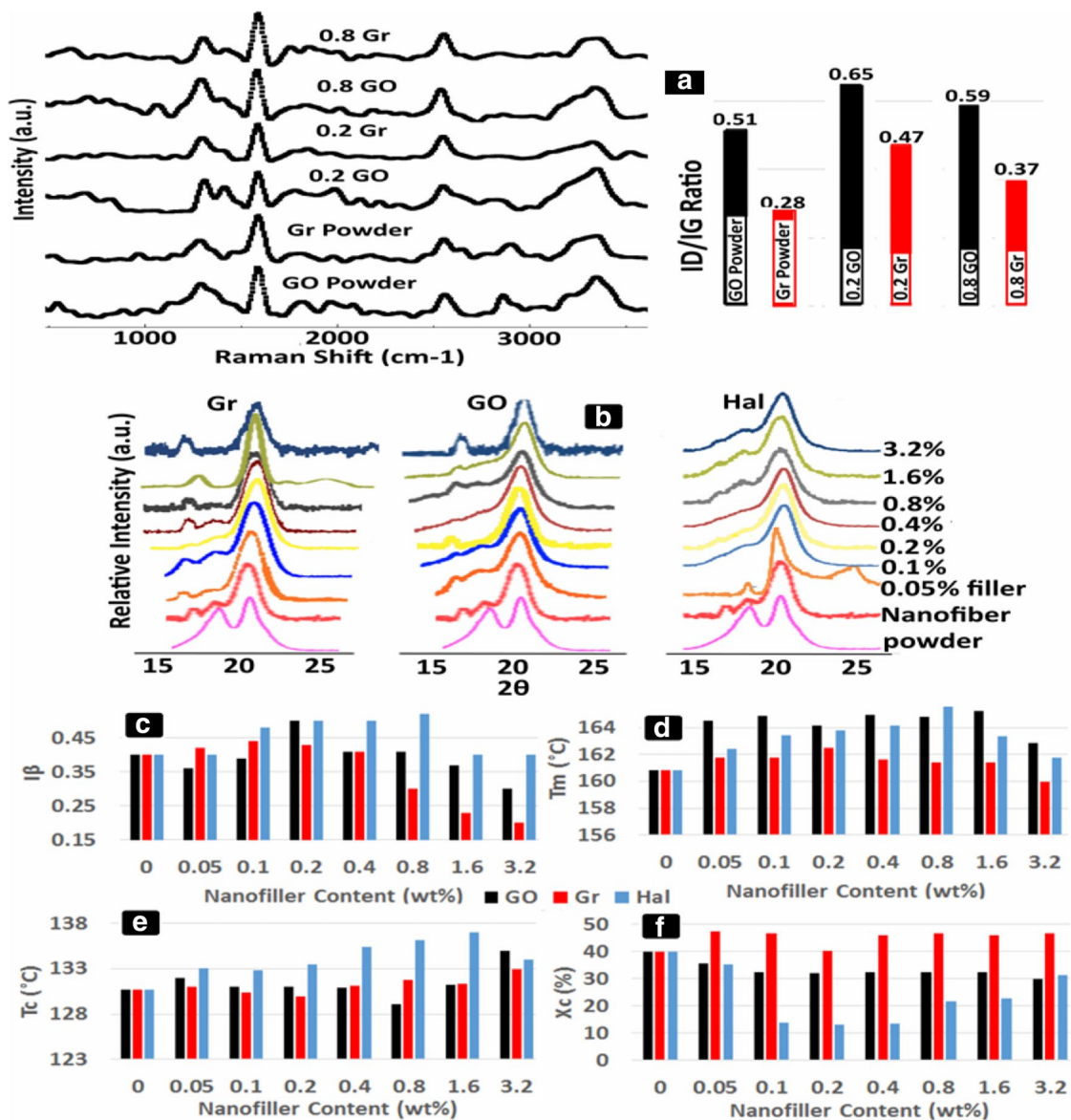


**Fig. 3** a Raman Spectrum and  $I_D/I_G$ , b XRD, c  $I_\beta$ , d  $T_m$ , e  $T_c$  and f  $X_c$  of PVDF nanofibers with different content of GO, Gr and Hal

peaks corresponding to structural defects (D band) and 1572–1608  $\text{cm}^{-1}$  peaks related to the vibration of  $\text{sp}^2$ -hybridized carbon (G band) were found in the Raman spectrum. The three peaks at 1298, 1587, and 2550  $\text{cm}^{-1}$  corresponded to the D-band, G-band, and 2D-band, respectively [47]. The observed blue-shift in the D-band from 2558  $\text{cm}^{-1}$  and 2554 in pure GO and Gr to approximately 2550  $\text{cm}^{-1}$  in PVDF/(0.2, 0.8) GO and PVDF/(0.2, 0.8) Gr samples, which also decreased in intensity, indicated that both GO and Gr flakes exfoliated in a PVDF polymer matrix [59].  $I_D/I_G$  of GO and Gr increased, which implies that the  $\text{SP}^2$  domain decreased upon interaction of GO and Gr with PVDF chains (Fig. 3a) [47].

The XRD pattern of different samples is shown in Fig. 3b. The characteristic peaks of the  $\alpha$ -phase, corresponding to the (100), (020), (110), and (021) planes, appeared at  $2\theta = 17.7^\circ$ ,  $18.6^\circ$ , and  $20.1^\circ$ . The diffraction peak of the  $\beta$ -phase, relating to the (200)/(110) plane, was observed at  $2\theta = 20.4\text{--}20.6^\circ$ . As  $I_\beta$  results show (Fig. 3c), the addition of fillers resulted in significant decreases in  $\alpha$ -polymorphism and greater increases in  $\beta$ -polymorphism of the PVDF. These results suggest that these different fillers played an important role in inducing the  $\beta$ -phase crystals, thereby retarding the crystallization of  $\alpha$ -phase [62]. The relative proportion of the  $\beta$ -phase in the XRD pattern increased with the filler additions, which had maximum value for 0.4 wt% Hal. The  $\beta$ -phase proportion decreased by approximately 11 and 19% for some concentrations of GO and Hal, respectively. This was due to beads formation and nanofillers aggregation in the PVDF nanofibers, which hindered the transformation of the PVDF crystal structures from  $\alpha$ - to the  $\beta$ -form and therefore decreased the piezoelectricity. The calculated values were also in good

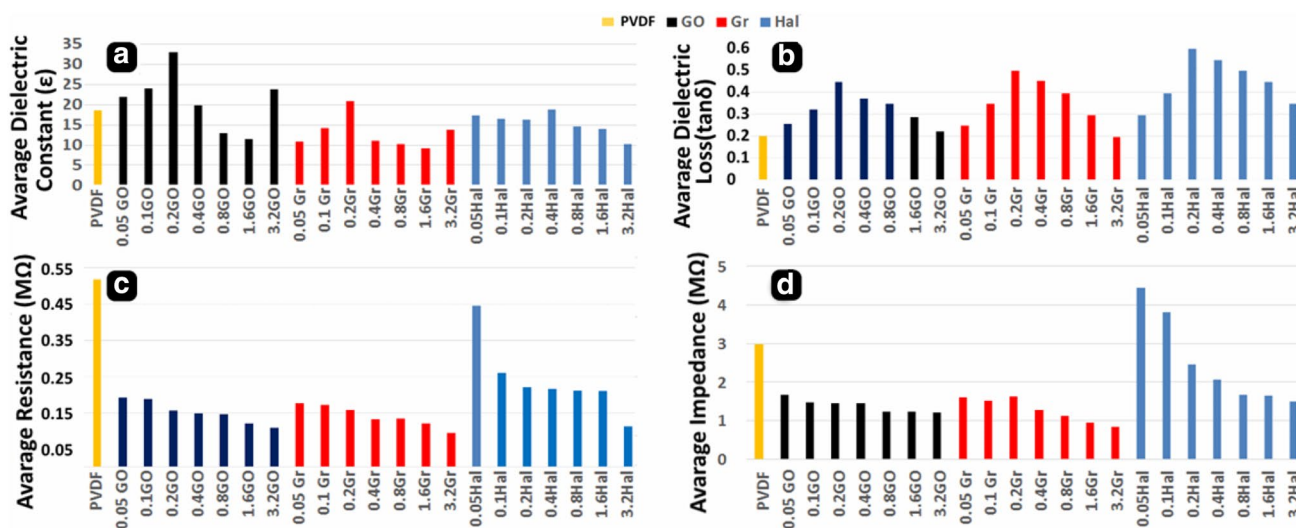
agreement with the values obtained from the FTIR analysis. Achaby et al. [62] found that the  $\alpha$ -peaks of PVDF nanocomposite films containing more than 0.075 wt% of GO content were totally disappeared, and a pure  $\beta$ -polymorph structure formed as well. They concluded that a 0.1 wt% of GO is sufficient to nucleate all PVDF chains into a  $\beta$ -phase. From the XRD and FTIR spectra, it was concluded that the  $\alpha$ -form dominated in the PVDF nanofibers. However, PVDF nanofibers containing added nanofillers had the most  $\alpha$ -form crystals convert to the  $\beta$ -form.

The DSC data show that the addition of different concentrations of GO, Gr, and Hal into the PVDF matrices caused the melting temperature ( $T_m$ ) and crystalline temperature ( $T_c$ ) to increase relative to the PVDF powder and pristine PVDF nanofibers (Fig. 3d–f). This result indicated that GO, Gr, and Hal acted as nucleating agents for the  $\beta$ -phase. However, the  $\Delta H_m$  and  $X_c$  values decreased after the addition of fillers, which confirmed that the presence of GO, Gr, and Hal significantly reduced the content of crystallinity caused by the  $\alpha$ -phase of the samples by hindering the movement of polymer chains of the  $\beta$ -PVDF [47].

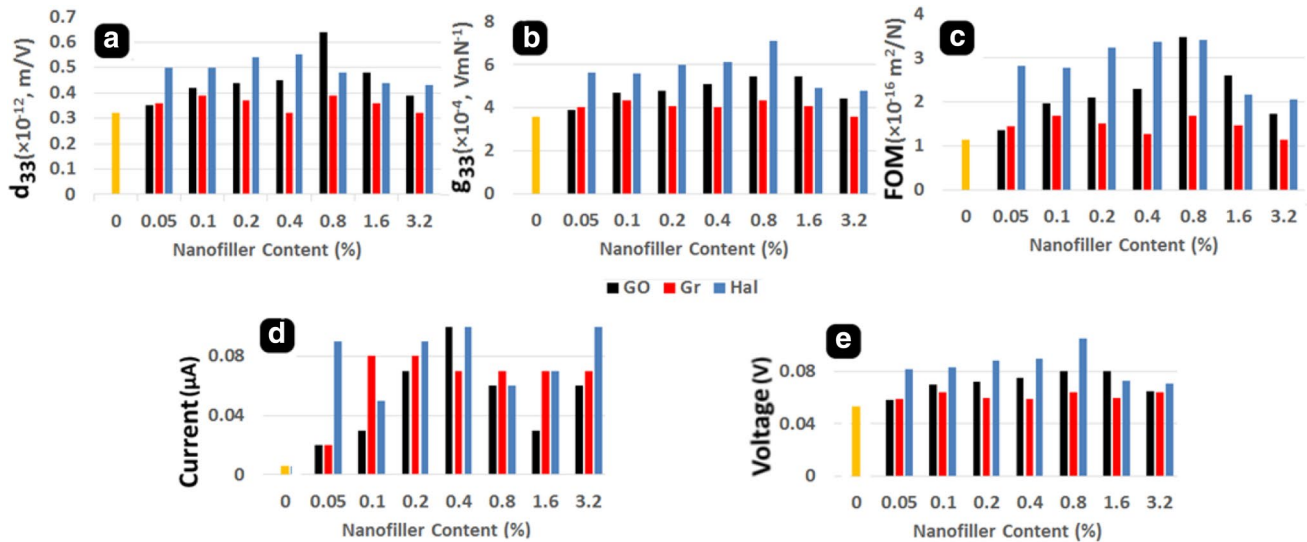
### 3.3 Dielectric properties and energy harvesting

Figure 4a shows the dielectric properties of samples with different content of nanofillers at room temperature and atmospheric pressure. The dielectric constant of PVDF nanofibers increased with nanofiller addition. But in the case of Gr and some concentration of Hal (0.8–3.2%) and GO (0.8 and 1.6%) the dielectric constant decreased which is due to aggregation and structural defects (beads).

The dielectric constant of the PVDF nanocomposite nanofibers showed typical percolation transition behavior



**Fig. 4** a Dielectric constant, b dielectric loss, c resistance, d impedance of pure PVDF and PVDF nanofibers with 0.05, 0.1, 0.2, 0.4, 0.8 and 3.2 wt% GO, Gr and Hal



**Fig. 5** Nanofiller content dependence of **a**  $d_{33}$ , **b**  $g_{33}$ , **c**  $FOM_{33}$ , **d** current and **e** voltage

as the content of doped nanofillers increased. As the results show, the dielectric constant of the PVDF nanocomposite fibers was enhanced as the nanofiller loading increased. The increase in the dielectric constant can be explained by the percolation theory (Eq. 8):

$$\epsilon = \epsilon_m(f_c - f)^{-s} \quad f < f_c \tag{8}$$

where  $\epsilon$  and  $\epsilon_m$  are the dielectric constants of the composites and the polymer matrix,  $f$  and  $f_c$  are the concentration and percolation threshold concentration of the filler in the matrix, respectively, and  $s$  is the scaling constant related to the materials' properties. Equation (8) indicates that  $\epsilon$  achieves a large value when  $f_{nanofiller} \rightarrow f_c$ . Therefore, the increase in the dielectric constant of nanofiller/polymer systems near the percolation threshold can be attributed to the microcapacitor effect. When the filler is placed between the isolated polymer chains, it forms many microcapacitor structures through the composite. The intensity of the local electric field then increases, which promotes both the migration and accumulation of charge carriers at the interface of the nanofiller and the PVDF matrix [63]. This interfacial polarization, which causes the enhancement of a dielectric constant, is explained by Maxwell–Wagner–Sillars [63]. The large polarization as well as the large dielectric constant occurs as the result of movement and accumulation of the charge carriers in the interface between nanofillers and the polymer matrix. The maximum dielectric constant was found to be 31, 22, and 18 for a 0.2 wt% addition of GO, Gr, and 0.4% addition of Hal, respectively. This was due to a higher accumulation of charge carriers at the PVDF/nanofiller interface. Electrical conductivity differences between the polymer and Hal and a large surface area of nanofiller lead to a higher possibility for the charge

carriers accumulating at the interface of the nanofiller and the PVDF matrix, which will result in more interfacial polarization as well as large dielectric constants [48].

The dielectric loss increased for nanofiller loading until it reached 0.2 wt%. Beyond 0.2 wt%, the dielectric loss of the PVDF nanocomposite fibers was found to decrease (Fig. 4b). The dielectric loss of nanocomposites mainly resulted from the  $\alpha$ -phase content in the PVDF matrices, whereas the fillers played an important role in reducing the  $\alpha$ -phase content of the PVDF. This indicates that the nanofillers disrupted the movements of the molecular chains of PVDF, which resulted in decreases in the dipole's loss [48].

The resistance and impedance of samples are represented in Fig. 4c, d. The resistance and impedance of Gr loaded samples had lower values than GO and Hal samples due to the higher conductivity of the Gr nanosheets.

Figure 5d, e show both current and output voltage of the samples when they were subjected to a repeated compressive impact (0.49 N). The electrical outputs were affected by filler content. Due to the  $\beta$ -phase increasing, the output voltage as well as the output current of all samples with different nanofillers was increased. The samples containing 0.8 Hal (0.1 V, 0.1  $\mu$ A) nanotube exhibited higher electrical output than GO (0.08 V, 0.07  $\mu$ A) and Gr (0.064 V, 0.1  $\mu$ A) due to rod like morphology and low viscosity (as SEM results show) which causes PVDF chains align in the electrospinning direction. From Eqs. 5, 6 and 7, it is concluded that the output voltage directly affected  $g_{33}$ ,  $d_{33}$  and  $FOM_{33}$ . The increase in output voltage in consequence of fineness and orientation of nanofibers caused the Hal samples showed higher  $d_{33}$  and  $g_{33}$  than GO and Gr (Fig. 5a–c). The higher values of  $FOM_{33}$  show the system higher efficiency to convert mechanical to electrical energy. It can be



concluded the Hal samples showed higher conversion efficiency than GO and Gr (5c).

## 4 Conclusion

In this study, graphene oxide, graphene nanosheets (as planar nanofillers) and halloysite nanotube were used to investigate the effect of nanofiller morphology on piezoelectric response. Electrospun PVDF nanocomposites including graphene oxide, graphene and halloysite nanotubes fabricated through electrospinning. The effect of nanofiller concentration as well as morphology on the formation of the electroactive phase responsible for the piezoelectric response were investigated. The  $\beta$ -phase and dielectric constant were increased by introducing nanofiller to PVDF matrix and they were in direct proportional with nanofiller properties. The graphene oxide caused the highest values of  $\beta$ -phase and dielectric constant among other fillers, due to more interaction of graphene oxide with PVDF matrix and its higher dielectric constant. It was concluded that for an electrospun PVDF nanocomposite, the piezoelectric response cannot be just evaluated with dielectric constant of nanofiller or  $\beta$ -phase percentage. Some other important factors such as orientation and fineness of electrospun nanofibers also play an important role in output voltage. The fibers fineness is even more important for nanocomposites because the nanostructuring of the fillers provoke relevant changes in the material structure and its final properties. For example, silicate nanotubes like chrysotile and halloysite make electrospun fibers straight and rigid and it could be very useful for the development of polymer piezoelectric materials. Therefore, PVDF/Hal nanocomposites fibers with lower dielectric constant showed more conversion efficiency or output voltage in compared with PVDF/GO, Gr nanocomposites.

## References

1. R. Khajavi, M. Abbasipour, *Piezoelectric PVDF Polymeric Films and Fibers: Polymorphisms, Measurements, and Applications* (Springer, New York, 2016), pp. 313–336
2. P. Martins, A.C. Lopes, S. Lanceros-Mendez, Electroactive phases of poly (vinylidene fluoride): determination, processing and applications. *Prog. Polym. Sci.* **39**, 683–706 (2014)
3. B. Mohammadi, A.A. Yousefi, S.M. Bellah, Effect of tensile strain rate and elongation on crystalline structure and piezoelectric properties of PVDF thin films. *Polym. Test.* **26**, 42–50 (2007)
4. H. Sobhani, M. Razavi-Nouri, A.A. Yousefi, Effect of flow history on poly (vinylidene fluoride) crystalline phase transformation. *J. Appl. Polym. Sci.* **104**, 89–94 (2007)
5. V. Sencadas, M.V. Moreira, S. Lanceros-Méndez, A.S. Pouzada, R. Gregório Filho, (2006)  $\alpha$ -to  $\beta$  Transformation on PVDF films obtained by uniaxial stretch. *Mater. Sci. Forum* **514**, 872–876
6. L. Li, M. Zhang, M. Rong, W. Ruan, Studies on the transformation process of PVDF from  $\alpha$  to  $\beta$  phase by stretching. *RSC Adv.* **4**, 3938–3943 (2014)
7. A. Salimi, A.A. Yousefi, Analysis method: FTIR studies of  $\beta$ -phase crystal formation in stretched PVDF films. *Polym. Test.* **22**, 699–704 (2003)
8. V. Sencadas, R. Gregorio Jr., S. Lanceros-Méndez,  $\alpha$  to  $\beta$  Phase transformation and microstructural changes of PVDF films induced by uniaxial stretch. *J. Macromol. Sci.* **48**, 514–525 (2009)
9. A. Ferreira, P. Costa, H. Carvalho, J.M. Nóbrega, V. Sencadas, S. Lanceros-Mendez, Extrusion of poly (vinylidene fluoride) filaments: effect of the processing conditions and conductive inner core on the electroactive phase content and mechanical properties. *J. Polym. Res* **18**, 1653–1658 (2011)
10. P. Sajkiewicz, A. Wasiak, Z. Gocłowski, Phase transitions during stretching of poly (vinylidene fluoride). *Eur. Polym. J.* **35**, 423–429 (1999)
11. B.E. El Mohajir, N. Heymans, Changes in structural and mechanical behaviour of PVDF with processing and thermo-mechanical treatments. 1. Change in structure. *Polymer* **42**, 5661–5667 (2001)
12. M. Mohammadzadeh, A.A. Yousefi, Deposition of conductive polythiophene film on a piezoelectric substrate: effect of corona poling and nano-inclusions. *Iran. Polym. J.* **25**, 415–422 (2016)
13. H. Pan, B. Na, R. Lv, C. Li, J. Zhu, Z. Yu, Polar phase formation in poly (vinylidene fluoride) induced by melt annealing. *J. Polym. Sci. B* **50**, 1433–1437 (2012)
14. B.S. Ince-Gunduz, R. Alpern, D. Amare, J. Crawford, B. Dolan, S. Jones, R. Kobylarz, M. Reveley, P. Cebe, Impact of nanosilicates on poly (vinylidene fluoride) crystal polymorphism: part 1. Melt-crystallization at high supercooling. *Polymer* **51**, 1485–1493 (2010)
15. D. Yang, Y. Chen,  $\beta$ -phase formation of poly (vinylidene fluoride) from the melt induced by quenching. *J. Mater. Sci. Lett.* **6**, 599–5603 (1987)
16. A. Grady, P. Sajkiewicz, S. Adamovsky, A. Minakov, S. Schick, Crystallization of poly (vinylidene fluoride) during ultra-fast cooling. *Thermochim. Acta* **461**, 153–157 (2007)
17. C. Ribeiro, V. Sencadas, J.L. Ribelles, S. Lanceros-Méndez, Influence of processing conditions on polymorphism and nanofiber morphology of electroactive poly (vinylidene fluoride) electrospun membranes. *Soft Mater* **8**, 274–287 (2010)
18. H.J. Chen, S. Han, C. Liu, Z. Luo, H.P. Shieh, R.S. Hsiao, B.R. Yang, Investigation of PVDF-TrFE composite with nanofillers for sensitivity improvement. *Sens. Actuator A* **245**, 135–139 (2016)
19. Y.K. Fuh, C.C. Kuo, Z.M. Huang, S.C. Li, E.R. Liu, A Transparent and flexible graphene-piezoelectric fiber generator. *Small* **12**, 1875–1881 (2016)
20. Z.H. Liu, C.T. Pan, L.W. Lin, H.W. Lai, Piezoelectric properties of PVDF/MWCNT nanofiber using near-field electrospinning. *Sens. Actuator A* **193**, 13–24 (2013)
21. A.C. Lopes, C.M. Costa, C.J. Tavares, I.C. Neves, S. Lanceros-Mendez, Nucleation of the electroactive  $\gamma$  phase and enhancement of the optical transparency in low filler content poly (vinylidene)/clay nanocomposites. *J. Phys. Chem. C* **115**, 18076–81802 (2011)
22. P. Martins, C. Caparros, R. Gonçalves, P.M. Martins, M. Benlemekki, G. Botelho, S. Lanceros-Mendez, Role of nanoparticle surface charge on the nucleation of the electroactive  $\beta$ -poly (vinylidene fluoride) nanocomposites for sensor and actuator applications. *J. Phys. Chem. C* **116**, 15790–15794 (2012)
23. Y. Wu, S.L. Hsu, C. Honeker, D.J. Bravet, D.S. Williams, The role of surface charge of nucleation agents on the crystallization

- behavior of poly (vinylidene fluoride). *J. Phys. Chem. B* **116**, 7379–7388 (2012)
24. D.H. Wang, W.H. Liao, Magnetorheological fluid dampers: a review of parametric modelling. *Smart Mater Struct* **20**, 023001 (2011)
  25. C. Chang, V.H. Tran, J. Wang, Y.K. Fuh, L. Lin, Direct-write piezoelectric polymeric nanogenerator with high energy conversion efficiency. *Nano Lett.* **10**, 726–731 (2010)
  26. Chan C., Fuh Y.K., Lin L.A., Direct-write piezoelectric PVDF nanogenerator, *Actuators and Microsystems, Conference 2009 Jun 21 IEEE*. PP. 1485–1488.
  27. H. Shao, J. Fang, H. Wang, T. Lin, Effect of electrospinning parameters and polymer concentrations on mechanical-to-electrical energy conversion of randomly-oriented electrospun poly (vinylidene fluoride) nanofiber mats. *RSC Adv* **5**, 14345–14350 (2015)
  28. A. Gheibi, M. Latifi, A.A. Merati, R. Bagherzadeh, Electrical power generation from piezoelectric electrospun nanofibers membranes: electrospinning parameters optimization and effect of membranes thickness on output electrical voltage. *J. Polym. Res.* **21**, 571 (2014)
  29. A. Gheibi, M. Latifi, A.A. Merati, R. Bagherzadeh, Piezoelectric electrospun nanofibrous materials for self-powering wearable electronic textiles applications. *J. Polym. Res.* **21**, 1–7 (2014)
  30. J. Fang, H. Niu, H. Wang, X. Wang, T. Lin, Enhanced mechanical energy harvesting using needleless electrospun poly (vinylidene fluoride) nanofiber webs. *Energy Environ. Sci.* **6**, 2196–2202 (2013)
  31. J. Fang, X. Wang, T. Lin, Electrical power generator from randomly oriented electrospun poly (vinylidene fluoride) nanofiber membranes. *J. Mater. Chem.* **21**, 11088–11091 (2011)
  32. Y. Ahn, J.Y. Lim, S.M. Hong, J. Lee, J. Ha, H.J. Choi, Y. Seo, Enhanced piezoelectric properties of electrospun poly (vinylidene fluoride)/multiwalled carbon nanotube composites due to high  $\beta$ -phase formation in poly (vinylidene fluoride). *J. Phys. Chem. C* **117**, 11791–11799 (2013)
  33. G.H. Kim, S.M. Hong, Y. Seo, Piezoelectric properties of poly (vinylidene fluoride) and carbon nanotube blends:  $\beta$ -phase development. *Phys. Chem. Chem. Phys.* **11**, 10506–10512 (2009)
  34. S. Yu, W. Zheng, W. Yu, Y. Zhang, Q. Jiang, Z. Zhao, Formation mechanism of  $\beta$ -phase in PVDF/CNT composite prepared by the sonication method. *Macromolecules* **42**, 8870–8874 (2009)
  35. Ou ZY, Liu ZH, Pan CT, Lin LW, Chen YJ, Lai HW Study on piezoelectric properties of near-field electrospinning PVDF/MWCNT nano-fiber. In *Nano/Micro Engineered and Molecular Systems (NEMS), 2012 7th IEEE International Conference on 2012 Mar 5* (pp. 125–128). IEEE.
  36. B. Li, C. Xu, J. Zheng, C. Xu, Sensitivity of pressure sensors enhanced by doping silver nanowires. *Sensor* **14**, 9889–9899 (2014)
  37. D. Shah, P. Maiti, E. Gunn, D.F. Schmidt, D.D. Jiang, C.A. Batt, E.P. Giannelis, Dramatic enhancements in toughness of polyvinylidene fluoride nanocomposites via nanoclay-directed crystal structure and morphology. *Adv. Mater.* **16**, 1173–1177 (2004)
  38. L. Priya, J.P. Jog, Poly (vinylidene fluoride)/clay nanocomposites prepared by melt intercalation: crystallization and dynamic mechanical behavior studies. *J. Polym. Sci. B* **40**, 1682–1689 (2002)
  39. Y.L. Liu, Y. Li, J.T. Xu, Z.Q. Fan, Cooperative effect of electrospinning and nanoclay on formation of polar crystalline phases in poly (vinylidene fluoride). *ACS Appl. Mater. Interfaces* **2**, 1759–1768 (2010)
  40. M.S. Bafqi, R. Bagherzadeh, M. Latifi, Fabrication of composite PVDF-ZnO nanofiber mats by electrospinning for energy scavenging application with enhanced efficiency. *J. Polym. Res.* **22**, 1–9 (2015)
  41. R.K. Layek, S. Samanta, D.P. Chatterjee, A.K. Nandi, Physical and mechanical properties of poly (methyl methacrylate)-functionalized graphene/poly (vinylidene fluoride) nanocomposites: piezoelectric  $\beta$  polymorph formation. *Polymer* **51**, 5846–5856 (2010)
  42. H.J. Kim, M. Noor-A-Alam, J.Y. Son, Y.H. Shin, Origin of piezoelectricity in monolayer halogenated graphene piezoelectrics. *Chem. Phys. Lett.* **603**, 62–66 (2014)
  43. J. Shang, Y. Zhang, L. Yu, B. Shen, F. Lv, P.K. Chu, Fabrication and dielectric properties of oriented polyvinylidene fluoride nanocomposites incorporated with graphene nanosheets. *Mater. Chem. Phys.* **134**, 867–874 (2012)
  44. S. Mohamadi, N. Sharifi-Sanjani, Investigation of the crystalline structure of PVDF in PVDF/PMMA/graphene polymer blend nanocomposites. *Polym Compos* **32**, 1451–1460 (2011)
  45. S. Ansari, E.P. Giannelis, Functionalized graphene sheet—Poly (vinylidene fluoride) conductive nanocomposites. *J. Polym. Sci. B* **47**, 888–897 (2009)
  46. A.A. Yousefi, Hybrid polyvinylidene fluoride/nanoclay/MWCNT nanocomposites: PVDF crystalline transformation. *Iran. Polym. J.* **20**, 25–733 (2011)
  47. S. Cho, J.S. Lee, J. Jang, Poly (vinylidene fluoride)/NH<sub>2</sub>-treated graphene nanodot/reduced graphene oxide nanocomposites with enhanced dielectric performance for ultrahigh energy density capacitor. *ACS Appl. Mater. Interfaces* **7**, 9668–9681 (2015)
  48. P. Thakur, A. Kool, B. Bagchi, S. Das, P. Nandy, Enhancement of  $\beta$  phase crystallization and dielectric behavior of kaolinite/halloysite modified poly (vinylidene fluoride) thin films. *Appl. Clay Sci.* **99**, 149–159 (2014)
  49. T. Huang, M. Lu, H. Yu, Q. Zhang, H. Wang, M. Zhu, Enhanced power output of a triboelectric nanogenerator composed of electrospun nanofiber mats doped with graphene oxide. *Sci. Rep* **5**, 13942 (2015)
  50. Z.Y. Jiang, G.P. Zheng, K. Zhan, Z. Han, J.H. Yang, Formation of piezoelectric  $\beta$ -phase crystallites in poly (vinylidene fluoride)-graphene oxide nanocomposites under uniaxial tensions. *J. Phys. D* **48**, 245303 (2015)
  51. P. Fakhri, H. Mahmood, B. Jaleh, A. Pegoretti, Improved electroactive phase content and dielectric properties of flexible PVDF nanocomposite films filled with Au- and Cu-doped graphene oxide hybrid nanofiller. *Synth. Met* **220**, 653–660 (2016)
  52. F. Mokhtari, M. Shamshirsaz, M. Latifi, S. Asadi, Comparative evaluation of piezoelectric response of electrospun PVDF (polyvinylidene fluoride) nanofiber with various additives for energy scavenging application. *J. Text. Inst.* **108**, 1–9 (2016)
  53. F. Akbar, M. Kolahtouz, S. Larimian, B. Radfar, H.H. Radamson, Graphene synthesis, characterization and its applications in nanophotonics, nanoelectronics, and nanosensing. *J. Mater. Sci. Mater. Electron.* **26**(7), 4347 (2015)
  54. Y. Zhu, S. Murali, W. Cai, Z. Li, J.W. Suk, J.R. Potts, R.S. Ruoff, Graphene and graphene oxide: synthesis, properties, and application. *Adv. Mater* **22**, 3906–3924 (2010)
  55. D. Rawtani, Y. Agrawal, Multifarious applications of halloysite nanotube: a review. *Rev. Adv. Mater. Sci* **30**, 282–295 (2012)
  56. D. Vatanserver, R.L. Hadimani, T. Shah, E. Siores, An investigation of energy harvesting from renewable sources with PVDF and PZT. *Smart. Mater Struct.* **20**, 055019 (2011)
  57. C.A. Martin, J.K. Sandler, M.S. Shaffer, M.K. Schwarz, W. Bauhofer, K. Schulte, A.H. Windle, Formation of percolating networks in multi-wall carbon-nanotube–epoxy composites. *Compos. Sci. Technol* **64**, 2309–2316 (2004)
  58. H.J. Lee, S. Zhang, Y. Bar-Cohen, S. Sherrit, High temperature, high power piezoelectric composite transducers. *Sensors* **14**, 14526–14552 (2014)
  59. M. Liu, B. Guo, Q. Zou, M. Du, D. Jia, Interaction between halloysite and 2,5-bis(2-benzoxazolyl) thiophene and their effects

- on reinforcement of polypropylene/halloysite nanocomposites. *Nanotechnology* **19**, 205709 (2008)
60. L. Wu, J. Xue, T. Itoi, N. Hu, Y. Li, C. Yan, J. Qiu, H. Ning, W. Yuan, B. Gu, Improved energy harvesting capability of poly (vinylidene fluoride) films modified by reduced graphene oxide. *J. Intell. Mater. System. Struct.* **25**, 1813–1824 (2014)
61. M.A. Rahman, B.C. Lee, D.T. Phan, G.S. Chung, Fabrication and characterization of highly efficient flexible energy harvesters using PVDF–graphene nanocomposites. *Smart Mater. Struct.* **22**, 085017 (2014)
62. M. El Achaby, M.K. Arrakhiz, S. Vaudreuil, E.M. Essassi, A. Qaiss, Piezoelectric  $\beta$ -polymorph formation and properties enhancement in graphene oxide–PVDF nanocomposite films. *Appl. Surf. Sci.* **258**, 7668–7677 (2012)
63. R. Moradi, J. Karimi-Sabet, M. Shariaty-Niassar, M.A. Koochaki, Preparation and characterization of polyvinylidene fluoride/graphene superhydrophobic fibrous films. *Polymers* **7**, 1444–1463 (2015)